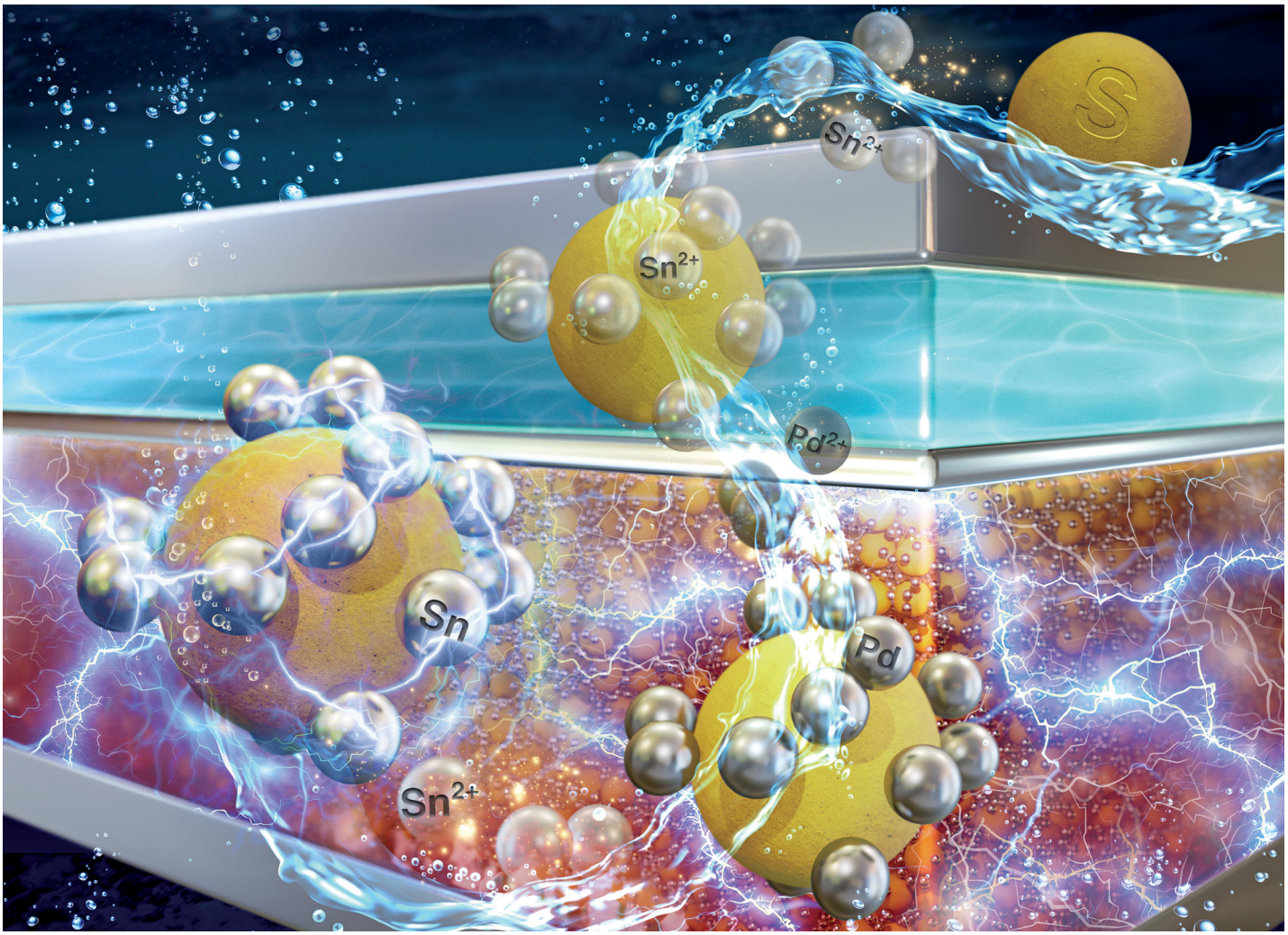

Showcasing research from Professor Sheng-Heng Chung's laboratory, Department of Materials Science and Engineering & Hierarchical Green-Energy Materials Research Center, National Cheng Kung University.

Electrolessly tin-plated sulfur nanocomposite for practical lean-electrolyte lithium–sulfur cells with a high-loading sulfur cathode

A nanosized tin-plating shell encapsulates a large amount of sulfur as an electrolessly tin-plated sulfur nanocomposite, exhibiting excellent electrochemical utilization and stability over a wide cycling rate at low electrolyte-to-sulfur ratios.

As featured in:

See Chui-Yi Kung and Sheng-Heng Chung, *Mater. Horiz.*, 2023, **10**, 4857.

ROYAL SOCIETY OF CHEMISTRY

rsc.li/materials-horizons

Registered charity number: 207890

Materials Horizons

ROYAL SOCIETY OF CHEMISTRY

COMMUNICATION

View Article Online
View Journal | View Issue

Cite this: *Mater. Horiz.*, 2023, 10, 4857

Received 7th June 2023,
Accepted 4th September 2023

DOI: 10.1039/d3mh00871a

rsc.li/materials-horizons

Electrolessly tin-plated sulfur nanocomposite for practical lean-electrolyte lithium–sulfur cells with a high-loading sulfur cathode†

Chui-Yi Kung[a] and Sheng-Heng Chung *[ab]

Lithium–sulfur batteries are among the most promising low-cost, high-energy-density storage devices. The high-capacity sulfur active material undergoes electrochemical conversion between the solid and liquid states. Thus, the comprehensive design of a suitable synthesis method, substrate material, and cathode configuration is essential for developing advanced sulfur cathodes with practical cell design and cell performance parameters. Herein, an electroless plating method is employed to develop a tin-plated sulfur nanocomposite. The nanosized tin plating shell effectively encapsulates a large amount of sulfur; the nanocomposite exhibits excellent high sulfur loading and content (6–10 mg cm^{-2} and 65–85 wt%, respectively), and the cell based on the nanocomposite exhibits a superior low electrolyte-to-sulfur ratio of 7–4 μL mg^{-1}. In addition to these critical cell design parameters, the tin-plated sulfur nanocomposite attains outstanding electrochemical utilization and stability for 200 cycles under a broad range of cycling rates of C/20–C/2, and additional outstanding cell performance properties in terms of a high areal capacity of 6.3–11.4 mA h cm^{-2}, a high gravimetric capacity of 520–663 mA h g^{-1}, a high energy density of 13–24 mW h cm^{-2}, and a low electrolyte-to-capacity ratio of 3.75 μL mA h^{-1}.

New concepts

We designed a novel tin-plated sulfur energy-storage material by autocatalytically depositing a nanosized tin-plating shell on sulfur particles using innovative materials science techniques. The tin content in the tin-plated sulfur nanocomposite is adjusted by controlling the plating time, synthesis temperature, and concentration of the plating solution. The optimal tin-plated sulfur energy-storage material exhibits record performances in terms of the cell design parameters, *i.e.*, a high sulfur loading in the cathode (6–10 mg cm^{-2}) and low electrolyte-to-sulfur ratios in the cell (7–4 μL mg^{-1}), and in terms of the cell performance parameters, *i.e.*, an areal capacity of 11.4 mA h cm^{-2}, which is higher than the required value for powering electric vehicles (2–4 mA h cm^{-2}); a high gravimetric capacity (520–663 mA h g^{-1}); an energy density of 13–24 mW h cm^{-2}, which is superior or comparable to those of current oxide cathodes (10–15 mW h cm^{-2}); and an electrolyte-to-capacity ratio of 3.75 μL mA h^{-1}, which is lower than that required for research-grade lithium–sulfur cells (<5 μL mA h^{-1}). Overall, we have established a new concept for the design of a sulfur-based composite cathode that differs from the existing frameworks in terms of the material, synthesis method, and configuration and exhibits record performances in terms of both cell design and cell performance parameters.

The demand for high-capacity cathodes for lithium-ion batteries has triggered a great interest in the development of high-energy-density lithium–sulfur batteries. The lithium–sulfur battery cathode is based on earth-abundant and bio-friendly sulfur, which has a high charge storage capacity of 1675 mA h g^{-1}, which is attributable to the two-electron electrochemical conversion reaction between sulfur (S_8) and lithium sulfide (Li_2S_2/Li_2S). Thus, the sulfur cathode provides cells with a capacity 10 times that provided by insertion-type oxide cathodes (100–200 mA h g^{-1}) in current lithium-ion batteries.[1–4] However, insulating sulfur acts as the active material of the electrochemical conversion sulfur cathode, which results in high cell polarization and sluggish reaction kinetics. These limit the electrochemical utilization of sulfur.[4–6] During the discharge/charge processes of the lithium–sulfur cell, the sulfur cathode is converted into liquid-state lithium polysulfides (Li_2S_n, $4 \leq n \leq 8$) at 2.3 V, which precipitate as insulating lithium sulfide at 2.1 V. The liquid-state polysulfides easily dissolve in the electrolyte and diffuse out from the cathode, resulting in poor active material retention and discharge–charge efficiency. The formation of the insulating sulfide results in a high resistance in the cell, deteriorating the electrochemical utilization and reversibility of the cathode.[4–6]

[a] *Department of Materials Science and Engineering, National Cheng Kung University, No. 1, University Road, Tainan City 70101, Taiwan. E-mail: SHChung@gs.ncku.edu.tw*

[b] *Hierarchical Green-Energy Materials Research Center, National Cheng Kung University, No. 1, University Road, Tainan City 70101, Taiwan*

† Electronic supplementary information (ESI) available. See DOI: https://doi.org/10.1039/d3mh00871a

To address the poor electrochemical performance of the lithium–sulfur battery cathode, studies have mainly focused on developing novel sulfur-based cathode composites *via* suitable synthesis methods[6–10] with novel substrate materials[11–16] and design configurations.[17–23] Sulfur encapsulation within a substrate through thermal melting and carbon disulfide dissolution methods are effective approaches for obtaining molten sulfur and dissolved sulfur, respectively, which can diffuse into the porous space of the substrate materials.[7–10] However, the resulting nanocomposite particles are mainly covered by the remaining sulfur (*i.e.*, unmelted, undissolved, or unabsorbed sulfur), thereby necessitating the use of additional conductive carbon and resulting in low sulfur content in the cathode. Moreover, the nanocomposite preparation method is often time-consuming and involves high temperatures and toxic materials.[4–6] The commonly used host materials in the preparation of sulfur-based cathode composites are carbon, polymers, and oxides.[11–16] Carbon is characterized by high porosity, which allows it to accommodate sulfur, and this porosity also allows the hosted sulfur to sit in the conductive carbon matrix.[11–13] However, carbon materials have a non-functional surface, resulting in weak polysulfide retention and thus limited sulfur accommodation capacity. Thus, polymers and oxides have been proposed as host materials because of their polysulfide chemisorption capability, which further contributes to the conversion of the trapped polysulfides during the discharge/charge processes.[14–16] However, the use of polymers and oxides results in limited improvement of the conductivity of the sulfur-based nanocomposites; this necessitates the use of additional conductive carbon, which limits the sulfur loading and content of the cathode, both of which are important parameters for realizing high-energy-density sulfur cathodes.[4–6] Sulfur-based nanocomposites with different host materials possess different morphologies. A porous host configuration is suitable for accommodating the active material and absorbing the diffusing polysulfides.[17–19] Thus, studies have adopted porous current collectors, in preference to flat and heavy aluminum-foil current collectors, as the cell component.[20,21] An upper current collector, also called an interlayer, further blocks the free migration of the dissolved polysulfides.[22,23] However, the use of additional cell components reduces the sulfur content in the cathode, and the use of high-porosity host materials and cell components results in the rapid consumption of a large amount of electrolyte in the cell.[4–6,24] These further challenge the development of high-energy-density lithium–sulfur, which requires a high and stable utilization of a large amount of sulfur in the lean electrolyte with a low electrolyte-to-sulfur ratio. Moreover, although the required cell design progress would improve the feasibility of the lithium–sulfur technology, the high-loading sulfur cathode often encounters high resistance and strong polysulfide shuttling, and the lean-electrolyte cell shows poor lithium-ion transfer. The resulting poor cyclability results in low stability and short cycle life, which restricts the study and development of critical parameters for lithium–sulfur batteries to be practically viable.[20–26]

Here, we report an electrolessly tin-plated sulfur nanocomposite with a high sulfur loading as the energy storage material for a lean-electrolyte lithium–sulfur cell. The nanocomposite was prepared *via* optimization of the synthesis method, substrate material, and configuration of the sulfur-based composite cathode. In the existing preparation method, the sulfur-based nanocomposite often leaves a sulfur layer on the surface of the substrate material, leading to high resistance and continuous polysulfide diffusion. Considering this, we applied the electroless plating method to synthesize the sulfur-based nanocomposite and, for the first time, designed a tin-plated sulfur energy storage material. The tin-plated sulfur nanocomposite was prepared through the rarely reported electroless deposition method, which involves the autocatalytic deposition of tin metal onto the nonconductive surface of the insulating sulfur.[25,26] Thus, the tin-plated sulfur nanocomposite comprised a unique nanoparticle tin shell covering a sulfur core. This advanced synthesis method and nanocomposite configuration endowed the cathode with adjustable sulfur content and loading to achieve an optimal configuration with high sulfur content (65–85 wt%) in a high-loading sulfur cathode (6–10 mg cm^{-2}) and a lean-electrolyte cell with a low electrolyte-to-sulfur ratio (7–4 μL mg^{-1}). These promising cell design parameters, in turn, endowed the lean-electrolyte lithium–sulfur cell with high electrochemical utilization (*i.e.*, a high discharge capacity of 1070–1160 mA h g^{-1}) and cycle stability (*i.e.*, a long cycle life of up to 500 cycles). Overall, the excellent cell design and cell performance parameters resulted in a high areal capacity (6.3–11.4 mA h cm^{-2}), gravimetric capacity (520–663 mA h g^{-1}), and energy density (13–24 mW h cm^{-2}), and a low electrolyte-to-capacity ratio (3.75 μL mA h^{-1}). Therefore, we demonstrate the application of the electroless plating synthesis method for designing a novel tin-plated sulfur nanocomposite to achieve excellent cell design parameters (*i.e.*, a high sulfur loading of >5 mg cm^{-2}, a high sulfur content of >50 wt%, and a low electrolyte-to-sulfur ratio of <5 μL mg^{-1})[4–7,24] and outstanding cell performance

Sheng-Heng Chung

With ten years of experience in lithium-ion battery research, from being a student to a researcher, we have always been inspired by the high-ranking research with high novelty and record materials performance from a prestigious journal: Materials Horizons. It was our great pleasure to be recognized as the 2021 Outstanding Reviewer for the journal. We are looking forward to contributing more to the peer review, and also to proposing this research paper to demonstrate our novel research in lithium–sulfur battery technology, with which we aim to illuminate a new research direction for elevating advanced rechargeable battery systems from the horizon.

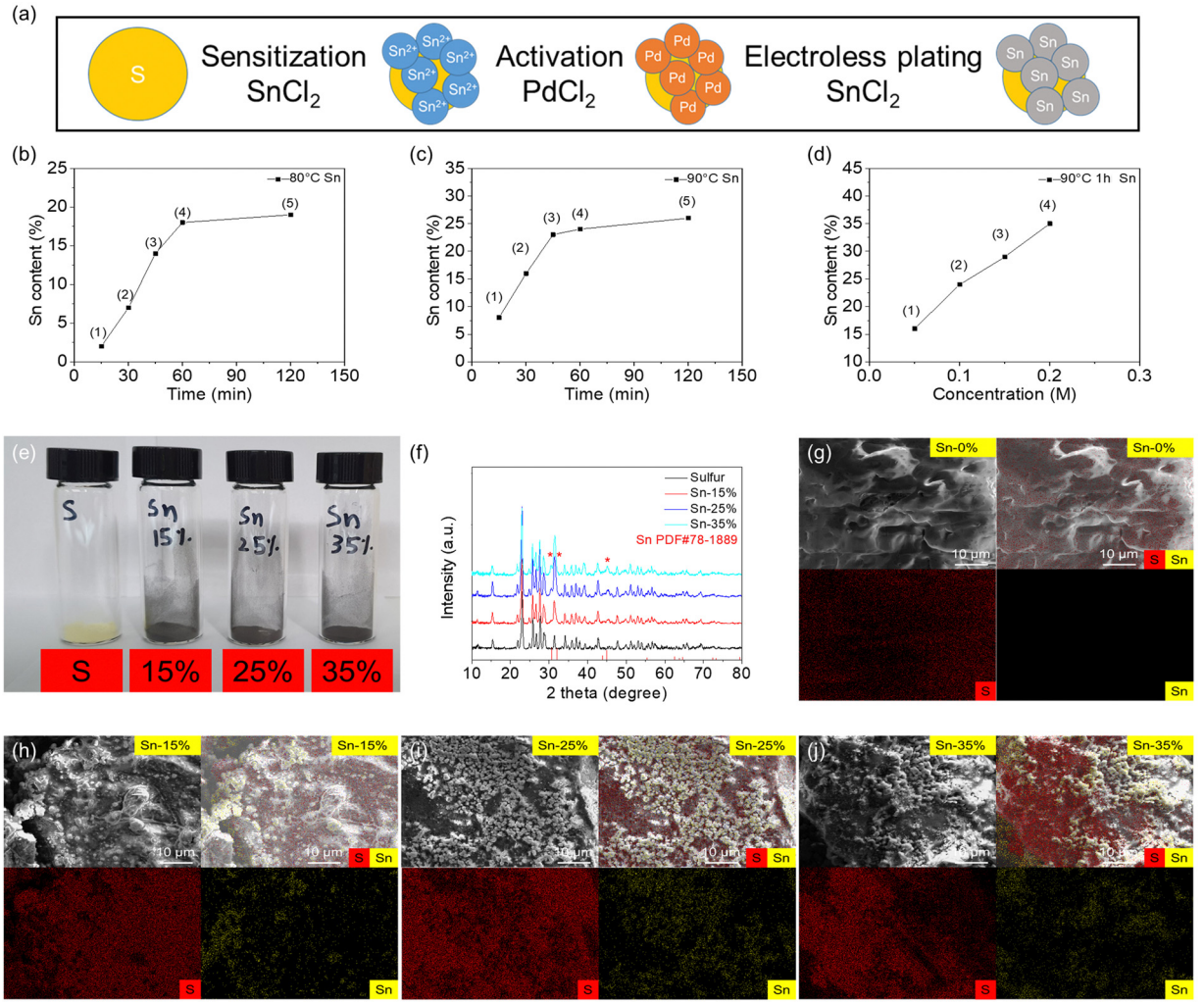

Fig. 1 Material characteristics. (a) Illustration of the synthesis of the tin-plated sulfur nanocomposite. The effects of time, temperature, and tin ion concentration on the tin plating amount during the electroless tin plating: (b) 80 °C and different plating times; (c) 90 °C and different plating times; and (d) 90 °C, 1 h, and different concentrations. (e) Photograph and (f) X-ray diffraction patterns of the sulfur and tin-plated sulfur nanocomposites. Scanning electron microscopy and energy-dispersive X-ray spectroscopy images of (g) sulfur and the tin-plated sulfur nanocomposites: (h) Sn-15%, (i) Sn-25%, and (j) Sn-35%.

values (*i.e.*, a high areal capacity of >4 mA h cm^{-2}, an energy density of >10 mW h cm^{-2}, and a low electrolyte-to-capacity ratio of <5 μL mA h^{-1}).[24–26]

Fig. 1 shows the material characteristics of the tin-plated sulfur nanocomposite synthesized *via* the electroless plating method under optimal conditions. The steps of electroless tin plating were divided into three main parts: sensitization, activation, and electroless plating. In this research, the commercial sulfur powder was immersed in $SnCl_2$ solution for sensitization to adsorb the divalent tin ions on the surface of sulfur particles. Then, the sensitized powder was immersed in $PdCl_2$ solution for activation. The divalent tin ions were replaced by metal palladium atoms, which formed active points to deposit metallic tin. Then, the activated powder was used to perform the electroless plating reaction, and the metallic tin was reduced on the surface of the sulfur particles to form the tin-plated sulfur nanocomposite (Fig. 1(a)). The electroless plating of tin onto the nonconductive sulfur involved an autocatalytic reaction, which was affected by the plating time and temperature and the concentration of the plating solution during the electroless plating.[25–28] Fig. 1(b)–(d) illustrates the effects of the plating time and temperature and the tin ion concentration of the plating solution. The autocatalytic reaction started at 80 °C under sufficient activation energy. With increasing plating duration from 15 to 120 min, the tin plating amount increased, and the highest amount ($\sim$20 wt%) was achieved at 60–120 min (Fig. 1(b) and Fig. S1a, ESI†). Achieving a higher tin plating amount required a higher plating temperature. Under a plating temperature of 90 °C, the tin plating amount increased from 10 to 25 wt% over time (Fig. 1(c) and Fig. S1b, ESI†). A higher plating temperature of over 90 °C led to violent catalysis reactions.[26–28] Thus, the influence of the tin ion concentration of the plating solution was explored at 90 °C by adjusting the concentration of the metallic salt (stannous

chloride) from 0.05 to 0.20 M. The obtained tin-plated sulfur nanocomposites showed tin plating amounts of 15, 25, 30, and 35 wt% for stannous chloride concentrations of 0.05, 0.10, 0.15, and 0.20 M, respectively (Fig. 1(d) and Fig. S1c, ESI†). We selected the tin-plated sulfur nanocomposites with 15, 25, and 35 wt% tin plating as our optimal samples, as the nanocomposites featured high tin plating amounts with well-controlled increases of 10 wt% and sufficient amounts of sulfur; the samples were named Sn-15%, Sn-25%, and Sn-35%, respectively. As shown in the photographs of the samples, the tin-plated sulfur nanocomposite changed from the yellow color of pure sulfur to the gray metal color of the tin shell (Fig. 1(e)). The material composition was determined *via* X-ray diffraction. The results showed pure sulfur and tin phases in the tin-plated sulfur nanocomposite. With increasing tin plating amount, the characteristic peaks of tin at 30.6°, 32.0°, and 44.9° increased, and no impurity peaks were detected. This indicates that pure tin was plated on the sulfur particles, and the purity of the sulfur core and the tin plating shell was not compromised (Fig. 1(f) and Fig. S2, ESI†). To determine the morphology of the nanocomposites, the microstructures and elemental compositions of the sulfur reference and the tin-plated sulfur nanocomposite were analyzed using scanning electron microscopy (SEM) and energy-dispersive X-ray spectroscopy (EDS). The tin-plated sulfur nanocomposite was composed of tin nanoparticles attached to micro-sized sulfur powder. With increasing salt concentration, the plated tin was deposited as nanoparticle clusters in the Sn-15% sample and as a tin plating shell in the Sn-25% and Sn-35% samples (Fig. 1(g)–(j)). Transmission electron microscopy (TEM) and the corresponding EDS elemental mapping results showed that the tin plating shell was uniformly dispersed on the large sulfur particles with different amounts of tin plating (Fig. S3, ESI†). The analytical results of SEM/EDS and TEM/EDS indicate that the tin-plated sulfur nanocomposite was successfully synthesized with the tin plating shell on the sulfur particle. Moreover, nitrogen adsorption–desorption isotherms were obtained to study the porosity of the tin-plated sulfur nanocomposites. The specific surface area and pore size distribution measurements indicated that both the sulfur and tin-plated sulfur nanocomposites had low specific surface areas of 0.01–3.74 $m^2\ g^{-1}$ and total pore volumes of 0.01–0.03 $cm^3\ g^{-1}$ (Fig. S4 and Table S1, ESI†). This implies that physical absorption due to large surface area and porous structures can be excluded from our case, and therefore, we would be able to focus on the chemical polysulfide adsorption of the tin plating shell. Considering that the tin content controlled both the sulfur content in the nanocomposite and the morphology of the sample, we analyzed the tin and sulfur contents and conducted thermogravimetric analysis, energy-dispersive X-ray spectroscopy analysis, elemental analysis, and true density analysis (Table S2, ESI†). The integrated analysis confirmed that Sn-15%, Sn-25%, and Sn-35% featured tin and sulfur contents of 13%–18% and 82%–85%, 21%–25% and 75%–78%, and 31%–38% and 62%–68%, respectively, affirming the high-accuracy control of the tin/sulfur content.

Fig. 2 summarizes the electrochemical and electrocatalytic characteristics of the tin-plated sulfur nanocomposites. The electrochemical impedance analysis of the high-loading sulfur cathode (6 mg cm^{-2}) based on the tin-plated sulfur nanocomposite revealed that the uncycled cells based on Sn-15%, Sn-25%, and Sn-35% achieved lower charge-transfer resistances (316, 224, and 173 Ω, respectively) than the cells based on sulfur (437 Ω), and the samples with lower resistance showed higher contents of metallic tin plating (Fig. 2(a), Fig. S5 and Table S3, ESI†). After cycling, the sulfur cathode and the tin-plated sulfur nanocomposites exhibited charge-transfer resistances and interfacial resistances of 55 Ω and 30 Ω and 21–24 Ω and 4–9 Ω, respectively (Fig. 2(b), Fig. S6 and Table S3, ESI†). The analytical results indicate that the metallic tin plating shell formed an electron-transfer network on the sulfur particle and between the nanocomposite particles. The addition of the metallic tin plating reduced the charge-transfer resistance of the uncycled cathode compared with that of the sulfur cathode, and the cycled tin-plated sulfur nanocomposite maintained a low charge-transfer resistance. The low interfacial resistance confirms that the tin plating shell blocked the fast diffusion of the dissolved polysulfides, which prevented the formation of an insulating deposit on the sulfur cathode, resulting in low interfacial resistance.[11,25–27] Moreover, the low impedance values of charge transfer and the interface in the freshly made and fully charged state of the cell suggest an internal mechanism that improves the lithium-ion diffusion due to the materials characteristics. Cyclic voltammetry (CV) analysis indicated that the pure sulfur cathode and the tin-plated sulfur nanocomposites featured the same cathodic and anodic reactions at 1.6–2.8 V, with no impurity-related redox peaks (Fig. 2(c)–(f)). The cell discharge curve featured two cathodic peaks, corresponding to the dissolution-conversion of solid-state sulfur into liquid-state polysulfides (cathodic peak [C1]) and the nucleation-conversion of liquid-state polysulfides into solid-state sulfide (C2). The reversible charge curve featured an anodic peak resulting from the dissolution of sulfide and its conversion into polysulfides and sulfur (anodic peak [A]).[29,30] The tin-plated sulfur nanocomposite showed a higher current and larger CV area than the sulfur cathode. The nanocomposite also featured higher polarization, because the tin plating shell allowed the nanocomposite to host a large amount of sulfur and adsorb a large amount of polysulfide. A large amount of active material, which is necessary to realize high energy density, often results in high polarization.[11–13,29,30] Although the polarization of the tin-plated sulfur nanocomposite was relatively high, the electrochemical reaction and reversibility were stable. Thus, the tin-plated sulfur nanocomposite showed large CV peaks and area even at a high scanning rate, indicating excellent electrochemical utilization and rate performance. Consequently, the tin-plated sulfur nanocomposites endowed the corresponding cells with high lithium-ion diffusion coefficients of 3.6×10^{-8}–1.6×10^{-7} (Sn-15%), 4.3×10^{-8}–2.1×10^{-7} (Sn-25%), and 5.5×10^{-8}–2.3×10^{-7} (Sn-35%) $cm^2\ s^{-1}$, which are higher than those of the cell based on the pure sulfur cathode (2.7×10^{-8}–1.5×10^{-7} $cm^2\ s^{-1}$; Fig. S7 and

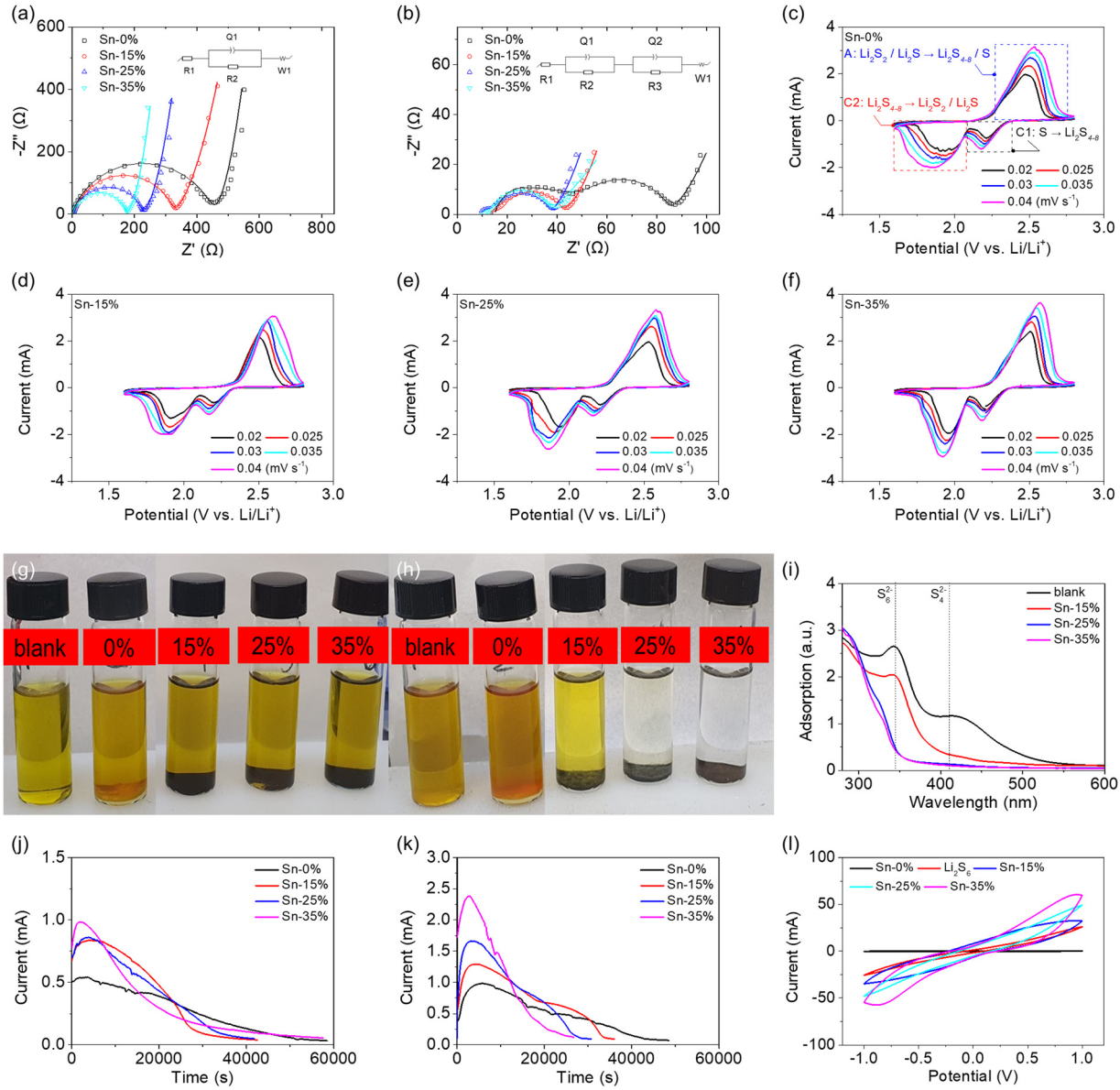

Fig. 2 Electrochemical and electrocatalytic characteristics. Electrochemical impedance spectra of the samples (a) before and (b) after cycling. Cyclic voltammetry curves of (c) sulfur, (d) Sn-15%, (e) Sn-25%, and (f) Sn-35% at 0.02–0.04 mV s^{-1}. Polysulfide adsorption solutions (g) before and (h) after one week of resting. (i) Ultraviolet-visible spectra of the polysulfide adsorption solutions after one week of resting. Electrocatalytic analysis: (j) sulfide nucleation, (k) sulfide dissolution, and (l) polysulfide conversion.

Table S3, ESI†). Moreover, the lithium-ion diffusion coefficients slightly increase as the amount of tin increases. This suggests that the tin plating shell benefits the redox reaction by enhancing the charge transfer. In addition, the overall lithium-ion diffusion coefficients are higher than the values reported in the lithium–sulfur literature. This is because of the use of a high-loading sulfur cathode and the realization of high electrochemical utilization of sulfur, which results in a high peak current.[24–26,31–34] During the CV scanning, the tin-plated sulfur nanocomposites showed high lithium-ion diffusion coefficients, which might result from the diffusing polysulfides that are trapped by the conductive tin plating shell and serve as the catholyte to promote the lithium-ion diffusion during cycling. This might be the external mechanism for the high lithium-ion diffusion. This improved lithium-ion diffusion performance endowed the tin-plated sulfur nanocomposite with high electrochemical utilization and allowed the realization of a lean-electrolyte cell.

The polysulfide adsorption capacities of sulfur and the tin-plated sulfur nanocomposites were analyzed. The diluted polysulfide solution containing sulfur remained light-brown after one week, the solution containing Sn-15% changed from light-brown to light-yellow, while the originally light-brown solutions containing Sn-25% and Sn-35% became transparent (Fig. 2(g) and (h)). The transparent color of the polysulfide solutions of Sn-25% and Sn-35% indicates that the tin plating

shell prevented the loss of the active material in the nanocomposite and allowed for strong and high polysulfide adsorption. Moreover, the polysulfide adsorption was stable for a long period (one week). The sample solutions were retrieved for ultraviolet-visible spectroscopy analysis. The adsorption analysis showed that the intensities of the polysulfide peaks (340 and 410 nm, corresponding to S_6^{2-} and S_4^{2-}, respectively) decreased from the pure sulfur to the Sn-15% sample, and the peaks were nonexistent in the Sn-25% and Sn-35% samples (Fig. 2(i)). The analytical results for the polysulfide solution with the tin-plated sulfur nanocomposites confirm the effective and strong polysulfide adsorption of the tin plating shell, which suggested that the plated tin nanoparticles might suppress the polysulfide shuttling[35–38] and also indicate that the shell induced electrocatalytic activity.[14–16,35–37] During the discharge process, the tin plating shell could electrocatalyze the conversion of the trapped/stabilized polysulfides into sulfides, as was proven by the sulfide nucleation analysis (Fig. 2(j)). The sulfide nucleation analysis revealed that the higher amount of tin endowed the cathode with a shorter conversion time to reach the peak current as well as higher peak current and resulting integrated area, which confirms that the tin plating shell boosted the reaction kinetics and the electrochemical utilization of the sulfur core. Sulfide activation during the charge process was analyzed *via* sulfide dissolution analysis (Fig. 2(k)). Compared with the sulfur cathode, the tin-plated sulfur nanocomposite attained a higher peak current within a shorter time with increasing tin content, which confirms that the tin plating shell also contributed to the oxidation reaction and thus improved the discharge–charge efficiency. The electrochemical redox efficiency of the tin-plated sulfur nanocomposite was further evaluated using a symmetric cell with 0.2 M Li_2S_6 polysulfide (Fig. 2(l)). The cell with the tin-plated sulfur nanocomposite displayed a response current in the CV analysis and tended to feature a higher current with increasing tin content. This substantiates the electrocatalytic capability and strong conversion kinetics offered by the tin plating shell.

Fig. 3 illustrates the cell performance of the tin-plated sulfur nanocomposite. The voltage profiles of the reference cell with the sulfur cathode showed typical cell failure because of the high polarization caused by the insulating sulfur and the high sulfur loading of 6 mg cm^{-2} (Fig. 3(a)). However, the tin-plated sulfur nanocomposite with the same high sulfur loading showed integral discharge–charge curves with excellent electrochemical stability during a 100-cycle test (Fig. 3(b)–(d)). Consistent with the CV analytical results, the voltage profiles displayed an upper discharge plateau corresponding to sulfur-to-polysulfide dissolution, a lower discharge plateau corresponding to polysulfide-to-sulfide nucleation, and integral charge curves with one overlapping charge plateau corresponding to reversible sulfide–polysulfide–sulfur conversion. However, as compared to the CV analysis, which was conducted at a relatively low scanning rate at 0.02–0.04 mV s^{-1}, the discharge and charge reaction was analyzed at a high rate of C/10 with a current density of 167.5 mA g^{-1}. As a result, the reference cell faces the diffusion of polysulfides and their re-deposition as insulating material in the cell, which results in the short upper discharge plateau and high polarization in the lower discharge plateau. In sharp contrast, the tin-plated sulfur nanocomposite has the tin plating shell to trap and convert the polysulfides, which reaches a low and stable polarization. Therefore, the voltage profiles confirm that the tin plating shell significantly reduced the polarization induced by the presence of a high amount of insulating sulfur in the cathode. Moreover, the tin plating shell maintained the active material in its conductive shell and thus enhanced the electrochemical utilization and stability of sulfur over a long cycle life of 100 cycles. The cycling performance of the tin-plated sulfur nanocomposite was analyzed with practical cell design parameters: a high sulfur loading of 6 mg cm^{-2}, a high sulfur content of 65–85 wt%, and a low electrolyte-to-sulfur ratio of 7 μL mg^{-1} (Fig. 3(e)). The cells with Sn-15%, Sn-25%, and Sn-35% achieved high discharge capacities of 1046, 1157, and 1155 mA h g^{-1}, respectively, which correspond to high electrochemical utilization of a large amount of sulfur (60–70%). After 100 cycles, the cells with Sn-15%, Sn-25%, and Sn-35% maintained high reversible capacities of 545, 662, and 705 mA h g^{-1}, respectively, which correspond to high capacity retention of 52–61%. The cycled cathodes retrieved from the cells were analyzed using SEM/EDS analysis. The microstructural and elemental analysis indicated strong elemental sulfur signals on the elemental tin signals, which agrees with the high retention and confirms the improved retention of the active material in the cathode and the stability of the tin-plated sulfur nanocomposite (Fig. S8, ESI†). In addition to exhibiting excellent electrochemical utilization and retention, the tin-plated sulfur nanocomposite displayed outstanding rate performance from C/20 to C/2 rate and high reversibility when the cycling rate was returned to C/10 rate after 100 cycles (Fig. 3(f) and Fig. S9, ESI†). The Sn-25% and Sn-35% samples exhibited similarly high cycling and rate performances. To further identify the practicability of the nanocomposites, we considered the capacity based on the electrodes. Sn-15%, Sn-25%, and Sn-35% achieved areal and gravimetric capacities of 6.3 mA h cm^{-2} and 565 mA h g^{-1}, 6.9 mA h cm^{-2} and 578 mA h g^{-1}, and 6.9 mA h cm^{-2} and 520 mA h g^{-1}, respectively. As shown in Fig. S10 (ESI†), a comparison of the gravimetric capacities of the cell with the tin-plated sulfur nanocomposite indicates that the Sn-25% sample exhibited the highest practical capacities and the highest electrochemical stability, which demonstrates its potential in endowing the lean-electrolyte cell with optimal cell design and cell performance parameters.

The optimal tin-plated sulfur nanocomposite, Sn-25%, showed excellent cyclability with a long cycle life of 200 cycles at various cycling rates from C/10 to C/2. The long-term rate performance aims to show the issue that a lean-electrolyte lithium–sulfur cell cycled with a high-loading sulfur cathode often encounters low lithium-ion transfer and high resistance, which results in high polarization. These issues together lead to irreversible capacity loss after few cycles and poor cyclability at high cycling rates. In our case, at cycling rates of C/10, C/5, C/3, and C/2, the cell with Sn-25% showed peak discharge and

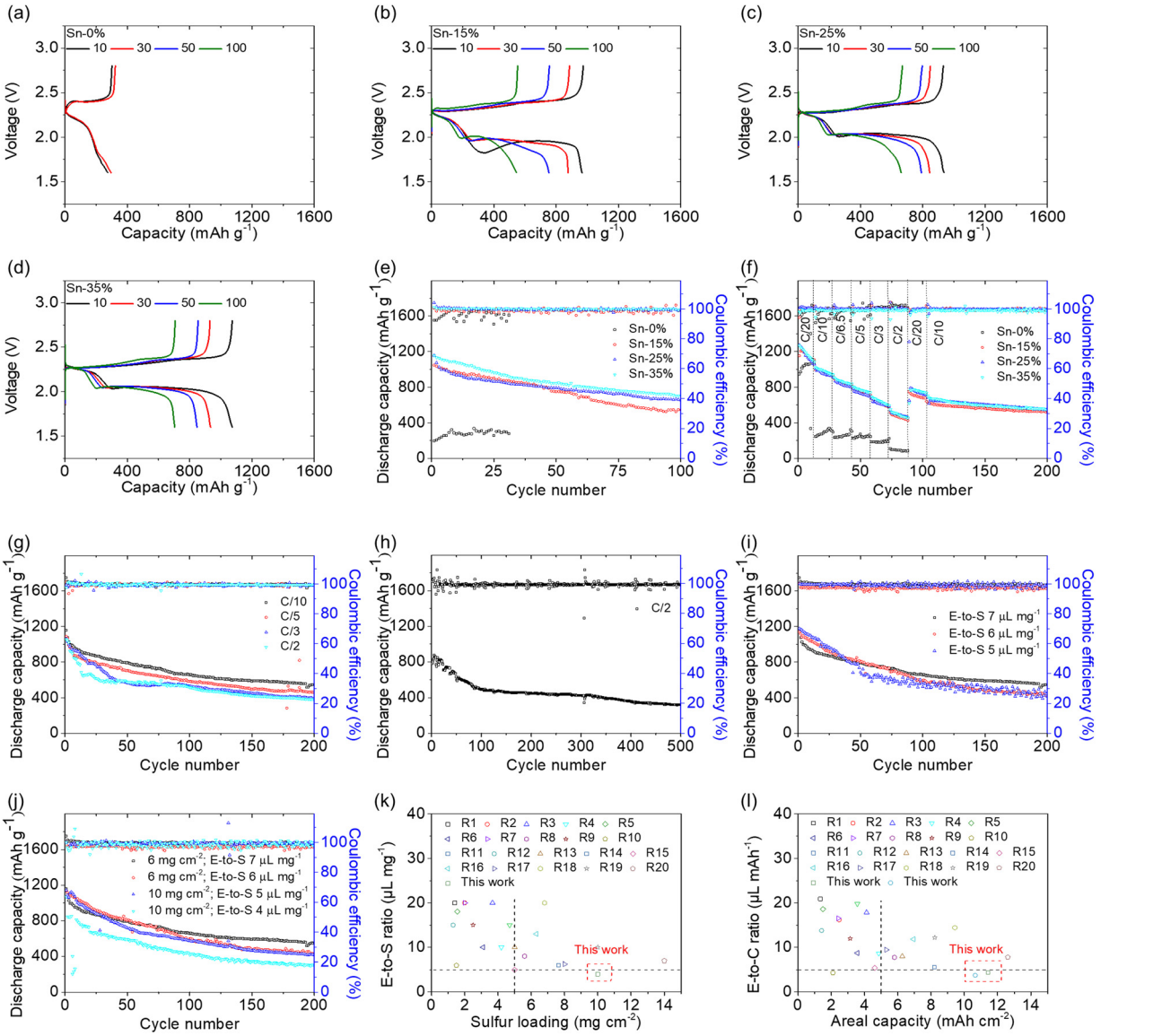

Fig. 3 Cell performance. Discharge–charge voltage profiles of (a) sulfur, (b) Sn-15%, (c) Sn-25%, and (d) Sn-35% at a C/10 rate for 100 cycles. (e) Cycling performance at a C/10 rate for 100 cycles and (f) rate performances of sulfur and tin-plated sulfur nanocomposites at C/20 to C/2. (g) Long-term rate performance, (h) long-term cycling performance, (i) lean-electrolyte testing, and (j) high-loading testing of Sn-25%. (k) Cell design parameters and (l) cell performance parameters of tin-plated sulfur nanocomposites compared with those of recent studies reporting metallic additives.

reversible capacities of 1157 and 547 mA h g^{-1}, 1089 and 460 mA h g^{-1}, 1064 and 390 mA h g^{-1}, and 1054 and 380 mA h g^{-1}, respectively, with high discharge–charge efficiencies of >99% (Fig. 3(g) and Fig. S11, ESI†). The tin-plated sulfur nanocomposite enables the lean-electrolyte lithium–sulfur cell to ameliorate these problems *via* the tin nanoshell with high conductivity, polysulfide adsorption, and electrocatalysis. Thus, our cell can maintain redox capability at a high rate and after many cycles. This improved electrochemical stability indicates high polysulfide retention at a low cycling rate and high reaction kinetics at a high cycling rate. Moreover, the cell with Sn-25% further demonstrated excellent long-term cyclability for 500 cycles at a C/2 rate with a low capacity fading rate of 0.12% per cycle (Fig. 3(h)). The Sn-25% also achieved a high rate performance from C/10, C/2, and 1C, reaching discharge capacities of 1159, 735, and 509 mA h g^{-1}, respectively (Fig. S12, ESI†). These confirm the enhanced electrochemical stability and reaction capability. At a 2C rate, a discharge capacity of 120 mA h g^{-1} results from the high polarization at high current density, which indicates that the optimal operation conditions of the tin-plated sulfur nanocomposite is a wide rate performance from a slow C/20 rate because of the improved polysulfide retention to a fast 1C rate because of the enhanced reaction kinetics. We next used X-ray photoelectron spectroscopy (XPS) to understand the adsorption and electrocatalysis of the tin plating shell. Fig. S13 (ESI†) shows the XPS analysis of Sn-25% before and after testing. The fresh Sn-25% showed the binding energy of S 2p at 165.0 eV and 163.9 eV, which are the

typical signals of sulfur, and the binding energy of Sn 3d at 495.4 eV and 486.9 eV, which are the typical signals of tin.[39–41] This confirms the formation of the tin plating shell on the sulfur particles of the Sn-25% (Fig. S13a and b, ESI†). The tested Sn-25%, which was intended to trap polysulfides, showed the binding energy of S 2p at 163.7 eV and 162.4 eV, which belong to polysulfides and the binding energy of Sn 3d at 495.8 eV and 487.3 eV, which belong to tin. The XPS analysis of the tested Sn-25% indicates that the tin plating shell is able to adsorb and assist in the reduction of the diffusing polysulfide with an increase in the Sn 3d peaks ($\sim$0.4 eV) (Fig. S13c and d, ESI†).[41–43] Moreover, the binding energy belonging to tin sulfides is not detected.[39,40] Therefore, the XPS analysis confirms that the tin plating shell was synthesized on the sulfur particles and benefited the polysulfide adsorption and conversion.

Furthermore, we explored the practicality of the tin-plated sulfur nanocomposite Sn-25% by reducing the low electrolyte-to-sulfur ratio and increasing the high sulfur loading step-by-step (Fig. 3(i), (j) and Fig. S14, S15, ESI†). With the increase in the insulating sulfur content of the cathode and the decrease in the lithium-ion-containing electrolyte, Sn-25% maintained excellent cyclability for 200 cycles under critical cell design conditions. Sn-25% provided the cell with 10 mg cm^{-2} sulfur and a 4 μL mg^{-1} electrolyte-to-sulfur ratio, and the cell achieved a high peak capacity of 1066 mA h g^{-1} and a high discharge–charge efficiency of >99%. Considering the large amount of sulfur and the low amount of electrolyte, the cell achieved outstanding electrochemical performance, including high areal and gravimetric electrode capacities of 10.7 mA h cm^{-2} and 618 mA h g^{-1}, respectively; a high energy density of 22.4 mW h cm^{-2}; and a low electrolyte-to-capacity ratio of only 3.7 μL mA h $^{-1}$, which easily meet the requirements for research-grade lithium–sulfur cells: an areal capacity of >4 mA h cm^{-2}, an energy density of >10 mW h cm^{-2}, and an electrolyte-to-capacity ratio of <5 μL mA h $^{-1}$.[4–7]

We next considered the current research progress in lithium–sulfur batteries that explore the scarcely reported metal substrates, and the application of metallic polysulfide adsorption and catalysis. In order to show the trend of development, we explored the critical cell design parameters considering the sulfur loading and electrolyte-to-sulfur ratio requirements of >5 mg cm^{-2} and <5 μL mg^{-1}, respectively. Our tin-plated sulfur nanocomposite exhibited a record high sulfur loading of 10 mg cm^{-2} and a low electrolyte-to-sulfur ratio of 4 μL mg^{-1} (Fig. 3(k) and Table S4, ESI†). Moreover, our tin-plated sulfur nanocomposite attained outstanding cell design and cell performance parameters, with low electrolyte-to-capacity ratios of 3.7 and 4.2 μL mA h^{-1}, which meet the requirement of <5 μL mA h $^{-1}$, while endowing the high-loading sulfur cathode with high areal capacities of 10.7 and 11.4 mA h cm^{-2}, which meet the requirement of >4 mA h cm^{-2} (Fig. 3(l) and Table S4, ESI†).[4–8,38,44]

The outstanding cell performance of the tin-plated sulfur nanocomposite inspired us to investigate the importance of the electroless plating method. Fig. 4 compares the material, electrochemical, and cell performances of Sn-25%, which is the tin-plated sulfur nanocomposite synthesized *via* the chemical method (*i.e.*, electroless plating), and S + Sn-25%, which is the sulfur–tin mixed composite prepared *via* the physical method (*i.e.*, mechanical mixing). The material analysis revealed the microstructural and elemental compositions of the tin-plated sulfur nanocomposite (*i.e.*, Sn-25%; Fig. 4(a)) and the sulfur/tin composite (*i.e.*, S + Sn-25%; Fig. 4(b)). The tin-plated sulfur nanocomposite comprised a uniform tin layer deposited on the sulfur particles, while the sulfur/tin composite comprised heterogeneously mixed sulfur and tin particles. The microstructural characteristics of the tin particles on the tin-plated sulfur nanocomposite and the sulfur/tin composite are shown in Fig. S16 (ESI†). The microstructural characteristics confirm that the tin-plated sulfur nanocomposite possessed nanosized tin particles plated on sulfur powder and clusters, resulting in a tight connection and good coverage. However, the tin particles in the sulfur/tin composite were micro-sized, and thus, it was difficult for the particles to closely connect with the micro-sized sulfur powder and clusters.

Furthermore, the electrochemical characteristics of the two samples were compared (Fig. 4(c)–(e)). The electrochemical impedance analysis showed that the addition of metallic tin to the sulfur cathode reduced the charge-transfer resistance of the cathode. The tin-plated sulfur nanocomposite provided a lower resistance (224 Ω) than the sulfur/tin composite (355 Ω) because of the close connection between the nanosized tin plating shell and the sulfur particles and between the nanocomposite particles (Fig. 4(c), Fig. S17 and Table S5, ESI†). The cycled cathodes based on the tin-plated sulfur nanocomposite showed low charge-transfer and interfacial resistances of 24 and 4 Ω, respectively, which were considerably lower than those of the sulfur/tin mixture-based cathode (47 and 32 Ω, respectively; Fig. 4(d), Fig. S18 and Table S5, ESI†). The low impedance of the tin-plated sulfur nanocomposite indicates excellent polysulfide retention and the electrocatalysis of the trapped polysulfides. The high impedance of the sulfur/tin composite indicates that the mixed micro-sized tin could not endow the sulfur clusters with a strong polysulfide adsorption capacity, and thus, the diffused polysulfides redeposited on the cathode and formed an insulating precipitate. The CV analysis showed that the CV peak current and integrated area of the sulfur/tin composite were lower than those of the tin-plated sulfur nanocomposite. This indicates the relatively limited improvement in the electrochemical utilization and efficiency of the sulfur/tin composite (*i.e.*, lithium-ion diffusion coefficient: 2.8×10^{-8}–1.3×10^{-7} cm^2 s^{-1}) compared with those of the tin-plated nanocomposite (*i.e.*, lithium-ion diffusion coefficient: 4.3×10^{-8}–2.1×10^{-7} cm^2 s^{-1}). The relatively low lithium-ion diffusion coefficient confirms that the sulfur/tin composite resulted in a small enhancement in the electrochemical utilization and rate capability (Fig. 4(e), Fig. S19 and Table S5, ESI†).[26,31–34]

The electrocatalytic characteristics of the two samples were first compared in terms of their polysulfide adsorption capacities. With the same content of tin in both composites, the tin-

plated sulfur nanocomposite displayed significantly weaker polysulfide peaks in its ultraviolet-visible spectrum than the sulfur/tin composite; moreover, the polysulfide solution of the tin-plated sulfur nanocomposite became transparent after one week of resting, while the sulfur/tin composite remained yellow (Fig. 4(f)). The results confirm the importance of the closeness of the nanosized tin plating with the sulfur powder for polysulfide adsorption and stabilization of the active material. Moreover, we conducted thermogravimetric analysis of the tin samples retrieved from polysulfide-adsorbed Sn-25% and S + Sn-25%. The weight losses of pure sulfur and tin, which were used as the reference baseline, were 100% and 0%, respectively; this demonstrates that any weight loss of the polysulfide-adsorbed samples was caused by sulfur decomposition. The tin retrieved from the polysulfide-adsorbed tin-plated sulfur nanocomposite exhibited a high weight loss, which indicates that the tin contained polysulfide, confirming that the high polysulfide adsorption of the nanocomposite was contributed by the nanosized tin (Fig. 4(g)). In contrast, the S + Sn-25% showed a low weight loss, which indicates weak polysulfide adsorption. Moreover, the electrocatalytic effect was studied according to the sulfide nucleation and dissolution reactions and the polysulfide conversion (Fig. 4(h)–(j)). Both the sulfide nucleation and dissolution reactions demonstrated that

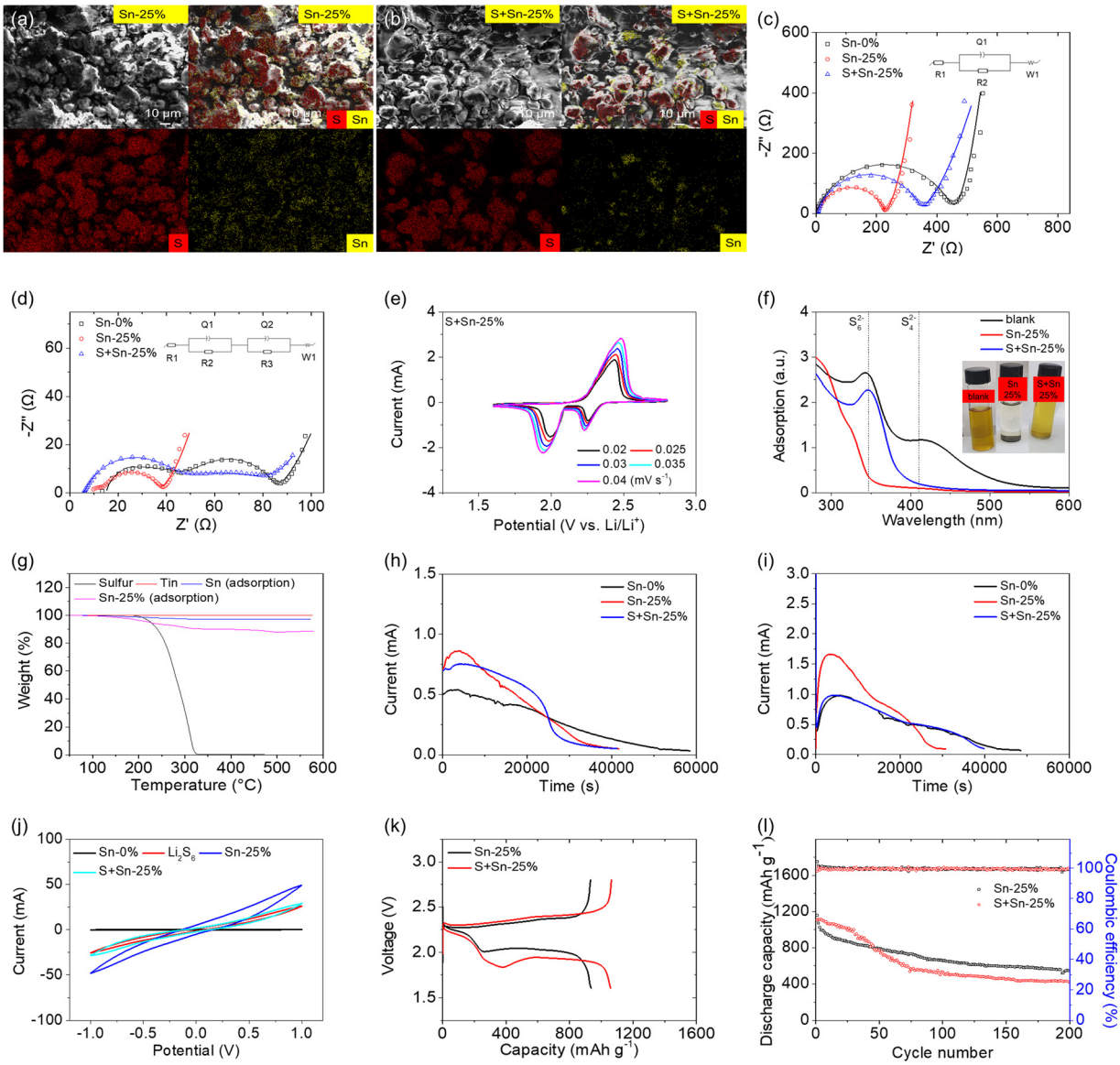

Fig. 4 Design of the synthesis method, substrate material, and configuration of the Sn-25% tin-plated sulfur nanocomposite and the S + Sn-25% sulfur/tin composite. Scanning electron microscopy and energy-dispersive X-ray spectroscopy images of (a) Sn-25% and (b) S + Sn-25%. Electrochemical impedance spectra of the samples (c) before and (d) after cycling. (e) Cyclic voltammetry analysis of S + Sn-25% at 0.02–0.04 mV s^{-1}. Polysulfide adsorption analysis: (f) ultraviolet-visible spectroscopy analysis of the polysulfide adsorption solution after one week of resting and (g) thermogravimetric analysis of the polysulfide-trapped tin. Electrocatalytic analysis: (h) sulfide nucleation, (i) sulfide dissolution, and (j) polysulfide conversion. (k) Discharge–charge voltage profiles and (l) cycling performances of Sn-25% and S + Sn-25% at a C/10 rate for 200 cycles.

the tin-plated sulfur nanocomposite required a shorter reaction time to reach a higher peak current than the sulfur/tin composite. This indicates that the nanosized tin particles and the molecular connection between the plated tin and the active material catalyzed the redox reaction during the polysulfide-to-sulfide conversion, which controls the main capacity output, and the sulfide-to-polysulfide conversion, which controls the charge reaction and the electrochemical efficiency of the cell (Fig. 4(h) and (i)). The symmetric cell based on the tin-plated sulfur nanocomposite exhibited a higher current than the sulfur/tin composite-based cell, which indicates that the nanocomposite exhibited a stronger electrocatalytic capability and faster conversion kinetics than the sulfur/tin composite (Fig. 4(j)).

The cell performances of the tin-plated sulfur nanocomposite and the sulfur/tin composite are illustrated in Fig. 4(k) and 4(l). The use of 25 wt% tin in the high-loading sulfur cathode benefited the electrochemical utilization. The tin-plated sulfur nanocomposite and the sulfur/tin composite achieved high discharge capacities of 1157 and 1106 mA h g^{-1}, respectively, and maintained high reversible capacities of 547 and 418 mA h g^{-1}, respectively. The corresponding discharge–charge voltage profiles also showed low polarization in the tin-plated sulfur nanocomposite (Fig. S20, ESI†). Thus, the cell performances agree with the material, electrochemical, and electrocatalytic analyses, which confirm that the tin-plated sulfur nanocomposite is the optimal composite cathode in terms of the synthesis method, substrate material, and configuration. The chemical synthesis provided a close connection between the tin nanoparticles and the sulfur powder. The nanosized tin provided the composite with strong polysulfide adsorption and electrocatalytic capability. The resulting nanosized tin plating shell resulted in excellent electron transport to enable the encapsulated active material to attain high electrochemical utilization and efficiency.

In conclusion, we propose a novel electrolessly tin-plated sulfur nanocomposite prepared based on the comprehensive optimization of the synthesis method, substrate material, and configuration of the sulfur-based composite cathode. The rarely reported electroless plating method allowed for the formation of a nanosized tin plating shell that covered the sulfur particles to encapsulate the active material and adsorb polysulfides. The tin nanoparticles formed an electron-transfer network on the sulfur particles and between the nanocomposite particles. Moreover, the tin nanoparticles demonstrated excellent polysulfide adsorption and electrocatalysis. The resulting nanocomposite configuration endowed the tin shell with improved active material accommodation and retention. Consequently, the tin-plated sulfur nanocomposite simultaneously achieved excellent cell design parameters (*i.e.*, a high sulfur loading [6–10 mg cm^{-2}], high sulfur content [65–85 wt%], and low electrolyte-to-sulfur ratio [7–4 μL mg^{-1}]) and cell performance parameters (*i.e.*, a high areal capacity [6.3–11.4 mA h cm^{-2}], high gravimetric capacity [520–663 mA h g^{-1}], high energy density [13–24 mW h cm^{-2}], and low electrolyte-to-capacity ratio [3.75 μL mA h^{-1}]). Therefore, the adopted electroless plating approach allows for the synthesis of novel tin-plated sulfur nanocomposites with a nanosized tin shell to improve the electrochemical performance of the high-loading sulfur cores in lean-electrolyte cells.

Conflicts of interest

There are no conflicts to declare.

Acknowledgements

This work is supported by the Ministry of Education (MOE) in Taiwan under Yushan Young Scholar Program and the National Science and Technology Council (NSTC) in Taiwan under grants 111-2636-E-006-027, 112-2636-E-006-006, and 111-2923-E-006-009. This research was supported in part by Higher Education Sprout Project, Ministry of Education to the Headquarters of University Advancement at National Cheng Kung University (NCKU). The authors gratefully acknowledge the use of EA000600, XRD005102, and ESCA000200 of MOST 111-2731-M-006-001 belonging to the Core Facility Center of National Cheng Kung University.

References

1 H. Li, Y. Li and L. Zhang, *SusMat*, 2022, **2**, 34–64.
2 A. Manthiram, J. L. Lutkenhaus, Y. Fu, P. Bai, B. G. Kim, S. W. Lee, E. Okonkwo and R. M. Penner, *One Earth*, 2022, **5**, 203–206.
3 S. Feng, Z.-H. Fu, X. Chen and Q. Zhang, *InfoMat*, 2022, **4**, e12304.
4 S. Tang, X. Li, Q. Fan, X. Zhang, D.-Y. Wang, W. Guo and Y. Fu, *J. Electrochem. Soc.*, 2022, **169**, 040525.
5 S.-H. Chung and A. Manthiram, *Adv. Mater.*, 2019, **31**, 1901125.
6 R. Deng, M. Wang, H. Yu, S. Luo, J. Li, F. Chu, B. Liu and F. Wu, *Energy Environ. Mater.*, 2022, **5**, 777–799.
7 S. Li and Z. Fan, *Energy Stor. Mater.*, 2021, **34**, 107–127.
8 L. Huang, J. Li, B. Liu, Y. Li, S. Shen, S. Deng, C. Lu, W. Zhang, Y. Xia, G. Pan, X. Wang, Q. Xiong, X. Xia and J. Tu, *Adv. Funct. Mater.*, 2020, **30**, 1910375.
9 R. Mori, *J. Solid State Electrochem.*, 2023, **27**, 813–839.
10 J. Li, L. Liu, J. Qi, Q. Qin, Q. Zhao, B. Wang and S. Zheng, *J. Porous Mater.*, 2022, **29**, 1727–1746.
11 Q. Xiao, J. Yang, X. Wang, Y. Deng, P. Han, N. Yuan, L. Zhang, M. Feng, C. Wang and R. Liu, *Carbon Energy*, 2021, **3**, 271–302.
12 A. Fu, C. Wang, F. Pei, J. Cui, X. Fang and N. Zheng, *Small*, 2019, **15**, 1804786.
13 A. I. Kamisan, T. I. T. Kudin, A. S. Kamisan, A. F. C. Omar, M. F. M. Taib, O. H. Hassan, A. M. M. Ali and M. Z. A. Yahya, *Int. J. Hydrogen Energy*, 2022, **47**, 8630–8657.
14 K. Liu, H. Zhao, D. Ye and J. Zhang, *Chem. Eng. J.*, 2021, **417**, 129309.
15 Q. Zhang, Q. Huang, S.-M. Hao, S. Deng, Q. He, Z. Lin and Y. Yang, *Adv. Sci.*, 2022, **9**, 2103798.

16 M. Zhang, W. Chen, L. Xue, Y. Jiao, T. Lei, J. Chu, J. Huang, C. Gong, C. Yan, Y. Yan, Y. Hu, X. Wang and J. Xiong, *Adv. Energy Mater.*, 2020, **10**, 1903008.
17 M. Wang, Z. Bai, T. Yang, C. Nie, X. Xu, Y. Wang, J. Yang, S. Dou and N. Wang, *Adv. Energy Mater.*, 2022, **12**, 2201585.
18 A. Benítez, J. Amaro-Gahete, Y.-C. Chien, Á. Caballero, J. Morales and D. Brandell, *Renewable Sustainable Energy Rev.*, 2022, **154**, 111783.
19 R. Fang, K. Chen, L. Yin, Z. Sun, F. Li and H. M. Cheng, *Adv. Mater.*, 2019, **31**, 1800863.
20 Y.-C. Ho and S.-H. Chung, *Chem. Eng. J.*, 2021, **422**, 130363.
21 L. Chen, H. Yu, W. Li, M. Dirican, Y. Liu and X. Zhang, *J. Mater. Chem. A*, 2020, **8**, 10709–10735.
22 D. Zhu, T. Long, B. Xu, Y. Zhao, H. Hong, R. Liu, F. Meng and J. Liu, *J. Energy Chem.*, 2021, **57**, 41–60.
23 Y.-C. Huang, Y.-J. Yen, Y.-H. Tseng and S.-H. Chung, *Molecules*, 2022, **27**, 228.
24 Y.-C. Wu and S.-H. Chung, *J. Mater. Chem. A*, 2023, **11**, 9455–9463.
25 C.-S. Cheng and S.-H. Chung, *Batteries Supercaps*, 2022, **5**, e202100323.
26 C.-S. Cheng and S.-H. Chung, *Chem. Eng. J.*, 2022, **429**, 132257.
27 J. G. M. Bremner, *Nature*, 1948, **162**, 183–184.
28 H. Niederprüm, *Angew. Chem., Int. Ed. Engl.*, 1975, **14**, 614–640.
29 C.-C. Wu and S.-H. Chung, *J. Power Sources*, 2023, **566**, 232944.
30 Y. V. Mikhaylik and J. R. Akridge, *J. Electrochem. Soc.*, 2004, **151**, A1969–A1976.
31 F.-N. Jiang, S.-J. Yang, H. Liu, X.-B. Cheng, L. Liu, R. Xiang, Q. Zhang, S. Kaskel and J.-Q. Huang, *SusMat*, 2021, **1**, 506–536.
32 X. Zhang, T. Yang, Y. Zhang, X. Wang, J. Wang, Y. Li, A. Yu, X. Wang and Z. Chen, *Adv. Mater.*, 2023, **35**, 2208470.
33 M. Zhao, P. Tan, D. Cai, Y. Liu, C. Zhang, B. Fei, B. Sa, Q. Chen and H. Zhan, *Adv. Funct. Mater.*, 2023, **33**, 2211505.
34 D. Lu, X. Wang, Y. Hu, L. Yue, Z. Shao, W. Zhou, L. Chen, W. Wang and Y. Li, *Adv. Funct. Mater.*, 2023, **33**, 2212689.
35 C. Zhou, Z. Li, X. Xu and L. Mai, *Natl. Sci. Rev.*, 2021, **8**, nwab055.
36 C. Zhou, M. Chen, C. Dong, H. Wang, C. Shen, X. Wu, Q. An, G. Chang, X. Xu and L. Mai, *Nano Energy*, 2022, **98**, 107332.
37 C. Dong, C. Zhou, Y. Li, Y. Yu, T. Zhao, G. Zhang, X. Chen, K. Yan, L. Mai and X. Xu, *Small*, 2023, **19**, 2205855.
38 G.-T. Yu and S.-H. Chung, *Small*, 2023, 2303490.
39 Y. Zhao, Z. Zhang, H. Dang and W. Liu, *Mater. Sci. Eng., B*, 2004, **113**, 175–178.
40 L. Luo, S.-H. Chung and A. Manthiram, *J. Mater. Chem. A*, 2018, **6**, 7659–7667.
41 D. Wang, Q. Cao, B. Jing, X. Wang, T. Huang, P. Zeng, S. Jiang, Q. Zhang and J. Sun, *Chem. Eng. J.*, 2020, **399**, 125723.
42 X. Yao, J. Xu, Z. Hong, G. Li, X. Wang, F. Lu, W. Wang, H. Liu, C. Liang, Z. Lin and W. Wang, *J. Phys. Chem. C*, 2018, **122**, 3263–3272.
43 Q. Shao, L. Xu, D. Guo, Y. Su and J. Chen, *J. Mater. Chem. A*, 2020, **8**, 23772–23783.
44 R. Fang, S. Zhao, Z. Sun, D. W. Wang, H. M. Cheng and F. Li, *Adv. Mater.*, 2017, **29**, 1606823.